Martini 3: a general purpose force field for coarse-grained molecular dynamics

Paulo Souza, Riccardo Alessandri, Jonathan Barnoud, Sebastian Thallmair, Ignacio Faustino, Fabian Grünewald, Ilias Patmanidis, Haleh Abdizadeh, Bart Bruininks, Tsjerk Wassenaar, et al.

Martini 3: A General Purpose Force Field for Coarse-Grained Molecular Dynamics

Paulo C. T. Souza*[1,2], Riccardo Alessandri[1], Jonathan Barnoud[1,3], Sebastian Thallmair[1,4], Ignacio Faustino[1], Fabian Grunewald[1], Ilias Patmanidis[1], Haleh Abdizadeh[1], Bart M.H. Bruininks[1], Tsjerk A. Wassenaar[1], Peter C. Kroon[1], Josef Melcr[1], Vincent Nieto[2], Valentina Corradi[5], Hanif M. Khan[5,6], Jan Domański[7,8], Matti Javanainen[9,10], Hector Martinez-Seara[9], Nathalie Reuter[6], Robert B. Best[8], Ilpo Vattulainen[10,11], Luca Monticelli[2], Xavier Periole[12,13], D. Peter Tieleman[5], Alex H. de Vries[1], Siewert J. Marrink*[1]

[1] Groningen Biomolecular Sciences and Biotechnology Institute and Zernike Institute for Advanced Material, University of Groningen, Nijenborgh 7, 9747 AG Groningen, The Netherlands.

[2] Molecular Microbiology and Structural Biochemistry, UMR 5086 CNRS & University of Lyon, 7 Passage du Vercors, F-69367, Lyon, France.

[3] Intangible Realities Laboratory, University of Bristol, School of Chemistry, Cantock's Close, Bristol BS8 1TS, United Kingdom.

[4] Frankfurt Institute for Advanced Studies, Ruth-Moufang-Str. 1, 60438 Frankfurt am Main, Germany.

[5] Centre for Molecular Simulation and Department of Biological Sciences, University of Calgary, 2500 University Drive NW, Calgary, Alberta T2N 1N4, Canada.

[6] Department of Chemistry and Computational Biology Unit, University of Bergen, N-5020 Bergen, Norway.

[7] Department of Biochemistry, University of Oxford, South Parks Road, Oxford OX1 3QU, United Kingdom.

[8] Laboratory of Chemical Physics, National Institute of Diabetes and Digestive and Kidney Diseases, National Institutes of Health, Bethesda, Maryland 20892-0520, United States.

[9] Institute of Organic Chemistry and Biochemistry, Czech Academy of Sciences, CZ-16610 Prague 6, Czech Republic.

[10] Computational Physics Laboratory, Tampere University, FI-33100 Tampere, Finland.

[11] Department of Physics, University of Helsinki, FI-00014 Helsinki, Finland.

[12] Department of Chemistry, Aarhus University, Aarhus C, Denmark.

[13] School of Biological Sciences, The University of Auckland, Symonds Street 3A, Auckland, New Zealand.

* Corresponding authors: Paulo C. T. Souza – paulocts@gmail.com
Siewert J. Marrink – s.j.marrink@rug.nl

ABSTRACT

The coarse-grained Martini force field is widely used in biomolecular simulations. Here, we present the refined model, Martini 3 (http://cgmartini.nl), with an improved interaction balance, new bead types, and expanded ability to include specific interactions representing, e.g. hydrogen bonding and electronic polarizability. The new model allows more accurate predictions of molecular packing and interactions in general, which is exemplified with a vast and diverse set of applications, ranging from oil/water partitioning and miscibility data to complex molecular systems, involving protein-protein and protein-lipid interactions and material science applications as ionic liquids and aedamers.

INTRODUCTION

The molecular dynamics (MD) simulation technique has become an indispensable tool in natural sciences, offering a spatio-temporal resolution unmatched by any experimental technique[1]. A major bottleneck of MD is the limited time and length scales that are accessible. To overcome this limitation, coarse-grained (CG) models representing groups of atoms by effective beads, have achieved widespread use[2]. The Martini model is among the most popular CG models in the field of biomolecular simulation, due to its easy-to-use building block principle. Martini relies on a four-to-one mapping scheme (i.e., on average four heavy atoms and associated hydrogens are mapped into one CG bead), and has been parametrized using a top-down approach with thermodynamic partitioning data as the main target[3,4]. Non-bonded interactions between neutral beads of Martini are solely described by

Lennard-Jones (LJ) potentials, while charged beads also include Coulombic interactions. The interaction strength of the LJ potential (i.e. its well depth) is used to discriminate between different levels of polarity of the CG beads. The model features four main classes of CG bead types, denoted C, N, P, and Q representing non-polar, intermediately polar, polar, and charged chemical groups, respectively[4]. Sub-labels are used to make a further distinction within a class in terms of degree of polarity or hydrogen donor/acceptor capabilities. In principle, all beads have the same size, denoted as regular (R) beads. By way of exception, special small (S) beads were introduced to model ring-like compounds for which a four-to-one mapping scheme is inadequate[4]. To reproduce correct stacking and hydrogen bonding distances between nucleotides, even smaller tiny (T) beads were found necessary[5]. Parametrization of the cross-interactions between S- and T-beads with R-beads, however, was done on an *ad-hoc* basis.

The Martini force field is used in a wide range of applications in diverse fields including structural biology[6–8], biophysics[9,10], biomedicine[11], nanotechnology[12,13], and materials design[14,15]. With its growing use, however, a number of shortcomings of the Martini model have recently been identified. One of the most important problems is the observation that certain molecules tend to interact too strongly. This has been reported for proteins and carbohydrates in solution, as well as for membrane embedded proteins[16–18]. The origin lies among others in small but systematic deviations in packing and intermolecular interactions[19]. Besides, the coverage of chemical space for broader applications was uneven, and in some cases, such as selectivity of nucleobase pairing[5,20], consistency was difficult to obtain given the limited

bead types and sizes. To alleviate these problems, we undertook a re-balancing of all non-bonded interaction terms of the Martini model, including the addition of new beads and labels. The new version, called Martini 3, enables more accurate simulations of molecular systems in general. In this paper, we present the key features of Martini 3 combined with examples of new applications and improvements in relation to the previous Martini model.

RESULTS

Re-parametrization of the beads. In Martini 3, the new parametrization strategy was based on the construction of prototype models of polar and non-polar molecules in all three Martini resolutions. Self- (R-R, S-S, and T-T) and cross-interactions (R-S, R-T, and S-T) of the different bead sizes were optimized to be well-balanced (**Supplementary Notes, sections B1 and B2**). In terms of chemical types, the beads were separated into three blocks: organic, ions, and water (**Supplementary Notes, section A1**). The organic (containing P-, N-, and C-beads) and ion (Q-beads) blocks have been subjected to independent parametrizations, where different trends in self-interaction, solvation, and transfer free energy upon bead size change were included (**Supplementary Notes, sections A1, B2,** and **B3**). In contrast to the previous version, water is defined as a separate bead type (called W), which enables optimization of water properties independently from other targets; for example, the freezing of water at room temperature (a problem sometimes encountered with the previous water model) no longer occurs. In addition, it is available in three different sizes as well (**Supplementary Notes, section B4**). Together with this optimization strategy, the new Martini 3 model

also features a fully revised interaction matrix (**Supplementary Notes, section A2**) and new intermediate interaction levels, added to smoothen the transition between chemical types (**Supplementary Notes, section A3**). Bead assignment and validation of the models were not only based on experimental transfer free energies, but also included solvent miscibility data (**Supplementary Notes, sections A6** and **C2,** and **Supplementary Results, sections E4-E6**) and a series of benchmark tests, ranging from structural properties of bilayers to dimerization potentials of mean force (PMFs) of proteins (**Methods, section 3**, **Supplementary Notes, section B5** and **Supplementary Results, sections F1-F5**).

The improved interaction balance between regular and smaller bead types is illustrated by the close to ideal mixing behavior of pure solvents composed of molecules mapped at different resolutions (**Fig. 1A**). Integration of radial distribution functions, defined as Kirkwood–Buff integrals (G_{ij}), are used here to quantify the degree of miscibility of the multi-resolution liquid water model (**Fig. 1B**). Theoretically, pair differences in Kirkwood–Buff integrals (ΔG_{ij}) should be equal to zero for all i,j pairs in ideal mixtures[21,22] while real mixtures that closely approach ideal behavior (like benzene-toluene) show values around ± 1 cm^3/mol[22]. Our multi-resolution water model shows $\Delta G_{ij} \approx -0.3$ cm^3/mol, indicating that the balance achieved with the new parametrization closely captures an ideal mixing behavior.

The accuracy of CG models containing ring or branched fragments, which rely heavily on smaller bead types, is also greatly increased in Martini 3. For example, the binary mixing behavior of various solvents (**Supplementary Results, sections E4-E6**) and the transfer free energies of many linear,

branched, and ring-like compounds (**Fig 1C** and **Supplementary Results, section E1**) are now in very good agreement with experimental data. The mean absolute error of transfer free energies compared to the experimental data is 2 kJ/mol, with 86% of the molecules presenting errors lower than 3 kJ/mol.

Another benefit of the recalibrated interactions is the disappearance of the artificially large desolvation free energy barriers that contribute to slow dissociation processes of the previous Martini 2 models. The problem, that was initially observed in dimerization of nucleobases[5,19], is thus solved, as highlighted by the comparison of Martini 2 and Martini 3 PMFs between cytosine and guanine (left panel of **Fig. 1D**). Note that there is room for further improvement, as the free energy minima of the CG PMF profiles with Martini 3 are shifted relative to the all-atom profiles because the bead sizes representing nitrogen-containing groups are not optimal to reproduce hydrogen bonding distances. In addition, the difference between C-G and G-G base pairs is not as large as in the atomistic case (~20 kJ/mol). However, it is still large enough (~8 kJ/mol) to provide specificity.

The proper balancing of R-, S-, and T-beads in Martini 3 also implies that the mapping choice of an arbitrary molecule to its Martini representation is now better defined. S- and T-beads are not only suited to represent ring-like compounds, but also used for cases involving 3-to-1 and 2-to-1 mapping of linear and branched chemical groups (**Supplementary Notes, section C1**).

Covering the chemical space with new beads and labels. Together with a thorough revision of the interaction strengths, in Martini 3, we extend the number of chemical bead types and the ability to modify the bead properties depending on the chemical details of the underlying moieties. Each P-, N-, and C-class now has 6 bead types with different degrees of polarity, which enables a more precise definition of different chemical groups by assigning them to certain bead types. Additionally, we introduce a new X-class of beads to model halo-compounds (**Supplementary Notes, section A1**). In the previous version of Martini, some of the bead types were already sub-classified according to their ability to act as hydrogen bond donor, acceptor, or both. This property can be now attributed to all bead types of intermediate or polar nature (N- or P- class). The effective interaction strength between donor and acceptor pairs is increased, whereas donor-donor and acceptor-acceptor pairs are weakened (**Supplementary Notes, section A4**). For example, Martini 3 correctly reproduces the trends in hydrogen bond-based pairing of nucleobases[5,20] without the use of special-purpose beads specifically for nucleobases (right panel of **Fig. 1D**). Note that chemical groups that can act as both donor and acceptor at the same time are always represented by the pure beads of the P- and N-class in Martini 3.

Next to the fine-tuning based on hydrogen bonding capabilities, we introduce the possibility to change the interactions based on the electronic polarizability. Depending on inductive or conjugate effects caused by chemical functionalization, non-polar molecules can be polarized, i.e., they can acquire an electron-donor (or “enriched”, label “e”) or electron-acceptor (or “vacancy”, label “v”) character, which can promote preferential interactions. Polarizable

groups in Martini 3 can be distinguished through the label “e/v” which can only be applied to the C- and X-class. A nice example of their application is the strong and specific interaction between electron donor and electron acceptor aromatic rings in aedamers, a class of molecules that have been studied extensively in the context of biomimetic folding and self-assembly[23,24]. The use of “e/v” allows Martini 3 to capture the preferential interaction between 1,5-dialkoxynaphthalene (DAN) and naphthalene diimide (NDI) (left panel of **Fig. 2A**) experimentally observed via NMR titration[23] and atomistic simulation data. Self-assembly of amide-linked tetramers shows preferential formation of alternating stacks of DAN and NDI, which is also measured by NMR and isothermal titration calorimetry investigations[24]. On top of hydrogen bonding and electron polarization labels, all beads can have their self-interaction fine-tuned by other sub-labels (as further described in the **Supplementary Notes, section A4**).

Chemical groups carrying monovalent charges +1/-1 are represented in Martini by the class of Q-beads (**Supplementary Notes, section A1**)**.** The original Martini model only considers monovalent ions, and was solely optimized for regular bead sizes which represented small ions and their first hydration shell. In Martini 3, charged groups can have either R-, S-, or T-size. The tiny size category allows modeling of small, bare ions, enabling applications that involve ion binding where (part of) the hydration shell is lost. This feature is exemplified by the binding of sodium ions (represented by a charged tiny bead) to a buried small cavity localized in the core of the adenosine A_{2A} receptor (**Fig. 2B**). X-ray crystallographic[25] and ligand binding assays[26] confirm the importance of sodium ions for the structure and for the

allosteric modulation of the A_{2A} receptor. Note that an extensive validation of the lipid models in Martini 3 was performed to allow simulations of transmembrane and peripheral membrane proteins (see **Supplementary Results, section F1**).

In addition to the smaller sizes, the Q-class was also expanded to five bead types, following the classical Hofmeister series trend[27,28] (**Supplementary Notes, section B3 and Supplementary Results, section F2**). At one extreme, the Q5 bead may be used to represent hard monovalent ions with the smallest polarizability, e.g. inorganic ions such as $R_2PO_4^-$. At the other end of the Martini Hofmeister series, the Q1 type models polarizable soft monovalent ions, like $N(CH_3)_4^+$, and implicitly includes in the LJ potential ion-π interactions. Such differences in behavior of the different Q-bead types are exemplified by MD simulations of the anion transfer between aqueous solutions and organophosphonium-based ionic liquids (**Fig. 2C and Supplementary Results, section F2**). Harder ions such as Cl^- (modeled as TQ5 with -1 charge) tend to stay in the water phase, together with Na^+ ions ($TQ5^+$ bead). In contrast, softer ions like ClO_4^- ($Q2^-$ bead) can exchange with Br^- ($SQ4^-$ bead) or (partially) PF_6^- ($Q1^-$ bead) from the ionic liquid phase. In the case of the biphasic system using trihexyltetradecylphosphonium bromide ($[P_{66614}][Br]$), direct comparison to experimental data shows good agreement for the anion transfer trends[28,29]. The new Q-bead types also impact biologically relevant systems, as exemplified by preferential cation-π interaction between choline groups ($Q1^+$ bead) of phosphatidylcholine lipids and aromatic residues of the *Bacillus thuringiensis* phosphatidylinositol-specific phospholipase C (*Bt*PI-PLC). In the previous version, such specific

252 interaction between soft ions and aromatic molecules were solely included in
253 the recently updated polarizable Martini implementation[30]. However, in Martini
254 3, the different Q-bead types allow easier (implicit) incorporation of such
255 interactions without the need for additional partial charges.

256 On top of the new chemical types, all Q-beads can use the hydrogen-bonding
257 labels (called in this case "p/n"). They represent organic charged molecules or
258 fragments, such as R-CH_2-COO^- and R-CH_2-NH_3^+, and also introduce
259 modifications in the Hofmeister trends of the pure Q-beads (**Supplementary**
260 **Notes, section A4**). Positively charged hydrogen donors ("p" label) interact
261 more strongly with non-polar beads, as expected in cation-π interactions. On
262 the other hand, negatively charged hydrogen acceptors ("n" label), have
263 stronger interactions with neutral polar beads, mimicking the stronger
264 hydrogen-bonds with anions. To complete the ion block, we explicitly include
265 a new D-bead for divalent ions (such as Ca^{2+}), which are typically hard ions.

266

267 **Improving packing and protein-protein interactions.** Another change in
268 philosophy with respect to the previous Martini models is the definition of
269 bonded interactions. Instead of using the center of mass of the mapped
270 chemical groups to define the geometry of the molecule, we now use a size-
271 shape concept aimed at preserving the volume of molecules in comparison to
272 all-atom reference structures. This choice and the proper use of Martini 3
273 bead sizes (**Supplementary Notes, sections C1 and C2**) lead to more
274 realistic molecular packing. As a consequence, the hydration of protein
275 pockets and channels is improved, as illustrated by the Fragaceatoxin C
276 (FraC) nanopore inserted in a lipid bilayer (**Fig. 3A**). The pore of FraC

remains open over the whole trajectory in Martini 3, as indicated by X-ray crystallography[31] and electro-osmotic flow assays[32], while in Martini 2 it is closed.

Another example of accurate packing is the stacking predictions of thiophene derivatives in bulk heterojunction solar cells composed of poly(3-hexyl-thiophene) (P3HT) and phenyl-C61-butyric acid methyl ester (PCBM) (**Fig. 3B**). The morphology of these organic solar cells is a determinant for high-efficiency devices[33]. The scattering profiles computed with Martini 3 show improved agreement with Martini 3 in relation to P3HT lamellar (peak around $q \approx 0.45$ Å^{-1}) and stacking ($q \approx 1.65$ Å^{-1}) experimental distances[33,34].

The use of bonds based on molecular volume and the appropriate choice of chemical bead types, sizes, and labels also controls the interaction density of the model, which has an important impact on the strength of collective interactions between molecules[19]. In order to test to what extent the changes in non-bonded and bonded interactions reduce the over-estimated aggregation of proteins, we performed extensive simulations comprised of solutions of soluble proteins as well as membrane embedded proteins. These systems were simulated under conditions in which proteins do not aggregate and, preferentially, stay as monomers. For soluble proteins (**Fig. 3C**), qualitative tests were performed with the headpiece domain of chicken villin[35], and the modified and mutated cellulose-binding domain from *Cellulomonas fimi* (EXG-CBM), which is an example of a protein completely free of charged side chains that can maintain solubility, stability, and function[36]. Trends are well-captured in Martini 3, with both proteins mainly staying as monomers in pure water (with only counter-ions to neutralize the system in the case of

villin). The villin headpiece showed salting-in behavior (i.e. less aggregation) under addition of 0.4M of NaCl, which was also observed for certain soluble proteins at low ionic strengths[37]. On the other hand, EXG-CBM only showed salting-out behavior (i.e. more aggregation), which was expected based on experimental data[36]. In contrast, both proteins aggregate in Martini 2, forming a single and stable aggregate during the simulation.

Polyleucine (K_2-L_{26}-K_2) was selected to evaluate the aggregation propensity in membranes. Experimental evidence with this transmembrane (TM) protein model indicates a preference for the monomeric state in a bilayer environment[38–40]. Both Martini 2 and 3 show that the hydrophobic mismatch between TM length and membrane thickness can play a role in the aggregation, with Martini 3 showing a higher percentage of the monomeric state (**Fig. 3D**). To quantitatively evaluate the strength of protein-protein interactions in a membrane environment, we also considered the dimerization of four selected transmembrane (TM) helices: the TM domains of the receptor tyrosine kinases EphA1 and ErbB1; the red blood cell protein glycophorin A (GpA); as well as the well-known model peptide WALP23 (left panel of **Fig. 3E**). For EphA1 and ErbB1, experimental dimerization free energies in a membrane environment have been estimated using Förster resonance energy transfer (FRET)[41,42]. For GpA, dimerization free energies range from around -15 kJ/mol (in various cell membrane environments)[43,44] to -31.5 kJ/mol (GALLEX assay in *E. coli* inner membranes)[45,46] or -50.6 kJ/mol (steric trap in POPC bilayers)[47]. WALP peptides have been characterized thoroughly during the past two decades, including their self-association[48]. For each one of the four peptide dimers, we compared experimental dimerization free energies

with the free energies predicted by the Martini 2 and Martini 3 model predictions. Martini 3 shows not only to be able to capture the correct trends, but also to quantitatively reproduce the experimental affinities. The binding mode also becomes improved as highlighted for GpA (right panel of **Fig. 3E**). The GpA homodimer structure with Martini 3 closely resembles experimental results obtained with NMR spectroscopy and crystallography[49–51].

In summary, for both soluble and transmembrane proteins, we observed that the Martini 3 models are in much better agreement with experimental data than before. Another advantage of the current Martini 3 protein model is that the default bead type representing the protein backbone in Martini 3 (a regular P2 bead) no longer depends on the secondary structure. In addition, the representation of protein flexibility can now be improved by the use of Gō-like models[52].

DISCUSSION

In this paper we have described the new version of the Martini force field, which shows numerous improvements in relation to the previous version. However, inherent limitations to the process of coarse-graining, related to transferability and representability problems[53–55] are still part of the model. An important drawback is the limited structural detail, that is a consequence of representing multiple atoms with isotropic interaction sites. This is most noticeable for the Martini water model, which represents four water molecules with a single LJ site and will certainly not capture any of the higher order structural correlations of real water. The role of explicit water in a CG model

such as Martini is mostly to provide a good solvent for polar compounds resulting in realistic partitioning. For applications requiring finer details, structure-based CG models are more suitable[56,57]. Another fundamental limitation is the entropy-enthalpy compensation. The loss of internal degrees of freedom for groups of atoms represented by a CG bead inevitably reduces the entropy of the system. Since the Martini force field is based on reproducing free energies, this requires a concomitant reduction in the enthalpy. As consequence, inaccurate entropy-enthalpy balance affects the temperature dependence of several properties and reduces the transferability to different state points. To probe transferability, we performed temperature dependent calculations for a number of solvent systems as well as lipid membranes (**Supplementary Results F**). Temperature dependent properties, like the heat expansion coefficient and heat capacity of water and n-octane, are very well captured by Martini 3, but this is not true for the hydrophobic effect, that shows the opposite trend with respect to atomistic models, in line with previous findings[58]. Note that the use of higher-resolution S- or T-particles does not remedy this problem, as these bead types were parameterized mainly to be compatible with the regular (R-type) beads and should be used primarily to represent parts of the system that cannot be adequately mapped with R-particles. Potential improvements with respect to the temperature transferability of our model could make use of environment dependent potentials[59] or CG beads with embedded sites, such as the polarizable water models[60,61], where incorporation of quadrupole moment might be required[58]. Bottom-up CG models that are derived with minimization of the information loss[54] as parameterization target might also perform better.

For a more in depth discussion of these and related issues with respect to the Martini coarse-graining philosophy, we refer to previous papers[62,63].

Keeping these limitations in mind, Martini 3 offers a versatile and easy to use generic force field to simulate molecular processes at a semi-quantitative level of accuracy. In relation to the previous model, the excessive over-estimated aggregation[19] is substantially reduced. We expect that Martini 3 will allow for more realistic predictions of protein interactions, as well as more accurate simulations of molecular systems in general. The increased number of bead types and interaction levels makes the model even more versatile, covering a larger part of chemical space with appropriate building blocks. Based on this new foundation, further optimizations for different classes of molecules are currently ongoing, including the use of Gō-potentials to alleviate limitations of protein conformational flexibility, a re-optimization of the bonded potentials of lipids and other biomolecular classes, as well as a compatible polarizable water model for applications requiring more realistic screening of electrostatic interactions. Finally, we foresee new application horizons for the Martini model in the field of materials science[64,65] and high-throughput drug design[66].

ONLINE CONTENT

Methods, including statements of data and code availability, supplementary information, and any other associated content and references, are available in the online version of the paper at https://doi.org/10.1038/sXXXXX-XXX-XXXX-X.

ACKNOWLEDGMENTS

We thank all members of the S.J.M. group and also external users for testing Martini 3 in its open-beta version. In particular, we would like to thank C.F.E. Schroer, P.W.J.M. Frederix, W. Pezeshkian, M.N. Melo, H.I. Ingólfsson, M. Tsanai, M. König, P. A. Vainikka, T. Zijp, L. Gaifas, J.H. van der Woude, M. Espinoza Cangahuala, M. Scharte, J. Cruiming, L.M. van der Sleen, V. Verduijn, A.H. Beck Frederiksen, B. Schiøtt, M. Sikora, P. Schmalhorst, K. Pluhackova, C. Arnarez, C.A. López, E. Jefferys, and M.S.P. Sansom for their preliminary tests with a lot of different systems including aedamers, sugars, amino acids, deep eutectic solvents, lipids, peptides, and proteins. We also thank the Center for Information Technology of the University of Groningen for providing access to the Peregrine high-performance computing cluster. We acknowledge the National Computing Facilities Foundation (NCF) of The Netherlands Organization for Scientific Research (NWO), CSC – IT Center for Science Ltd (Espoo, Finland), and CINES (France) for providing computing time. Work in the S.J.M. group was supported by an ERC Advanced Grant "COMP-MICR-CROW-MEM". R.A. thanks The Netherlands Organisation for Scientific Research NWO (Graduate Programme Advanced Materials, No. 022.005.006) for financial support. L.M. acknowledges the Institut National de la Santé et de la Recherche Medicale (INSERM) and the Agence Nationale de la Recherche (ANR) for funding (grant no. ANR-17-CE11-0003) and GENCI-CINES for computing time (grant no. A0060710138). S.T. acknowledges the support from the European Commission via a Marie Skłodowska-Curie Actions individual fellowship (MicroMod-PSII, grant agreement 748895). M.J. thanks the Emil Aaltonen foundation for financial

support. I.V. thanks the Academy of Finland (Center of Excellence program (grant no. 307415)), Sigrid Juselius Foundation, the Helsinki Institute of Life Science fellow program, and the HFSP (research grant Ref.-No: RGP0059/2019). R.B. and J.D. were supported by the intramural research program of the NIDDK, NIH. Their work utilized the computational resources of the NIH HPC Biowulf cluster. (http://hpc.nih.gov). H.M.-S. acknowledges the Czech Science Foundation (19-19561S). J.B. acknowledges funding from the TOP grant of S.J.M. (NWO) and the EPSRC program grant EP/P021123/1. Work in D.P.T.'s group is supported by the Natural Sciences and Engineering Research Council (Canada) and Compute Canada, funded by the Canada Foundation for Innovation. D.P.T. acknowledges further support from the Canada Research Chairs program.

AUTHOR CONTRIBUTIONS

P.C.T.S. and S.J.M. conceived the project with suggestions from R.A., A.H.V., J.B., and S.T.; P.C.T.S. generated and optimized all bead parameters; P.C.T.S., R.A., and J.B. generated the topology and bonded parameters of all CG models with suggestions from S.T. and I.F.; P.C.T.S., R.A., A.H.V., and F.G. performed the simulations and analysis involving transfer free energies, solvent and polymer properties; P.C.T.S., S.T., J.B., and J.M. performed the simulations and analysis involving lipid bilayers; P.C.T.S., I.F., and R.A. performed the simulations and analysis involving nucleobases; P.C.T.S., I.P., and A.H.V. generated the models, performed the simulations and analysis involving aedamers; P.C.T.S., and F.G. generated the models, performed the simulations and analysis involving ionic liquids and ionic water solutions; R.A.

generated the models, performed the simulations and analysis involving bulk heterojunctions, with suggestions from L.M. regarding the fullerene model; P.C.T.S., J.B., H.A., R.A., B.M.H.B., S.T., J.M., V.N., X.P., M.J., H.M.K., J.D., V.C., and H.M.-S. performed the simulations and analysis involving amino acids, peptides and proteins; J.B., T.W., P.K., and S.T. developed some tools and scripts used to generate the CG models and to run the MD simulations; L.M., R.B., P.T., N.R., I.V., A.H.V., and S.J.M. provided guidance and supervision in the studies performed by their respective group members and collaborators; P.C.T.S. and S.J.M. wrote the main manuscript, with contributions from all the authors; P.C.T.S. prepared the figures with contributions from R.A., B.M.H.B., H.M.K., and A.H.V.; P.C.T.S. wrote the Methods with contributions from all the authors. P.C.T.S. wrote the Supplementary Information, with contributions from all the authors. All the authors revised and approved the final version of the manuscript, Online Methods, and Supplementary Information.

COMPETING INTERESTS

The authors declare no competing interests.

REFERENCES

1. Bottaro, S. & Lindorff-Larsen, K. Biophysical experiments and biomolecular simulations: A perfect match? *Science* **361**, 355–360 (2018).

2. Ingólfsson, H. I. *et al.* The power of coarse graining in biomolecular simulations. *Wiley Interdiscip. Rev. Comput. Mol. Sci.* **4**, 225–248 (2014).

3. Marrink, S. J., De Vries, A. H. & Mark, A. E. Coarse Grained Model for Semiquantitative Lipid Simulations. *J. Phys. Chem. B* **108**, 750–760 (2004).

4. Marrink, S. J., Risselada, H. J., Yefimov, S., Tieleman, D. P. & de Vries, A. H. The MARTINI force field: coarse grained model for biomolecular simulations. *J. Phys. Chem. B* **111**, 7812–7824 (2007).

5. Uusitalo, J. J., Ingólfsson, H. I., Akhshi, P., Tieleman, D. P. & Marrink, S. J. Martini Coarse-Grained Force Field: Extension to DNA. *J. Chem. Theory Comput.* **11**, 3932–3945 (2015).

6. Abellón-Ruiz, J. *et al.* Structural basis for maintenance of bacterial outer membrane lipid asymmetry. *Nat. Microbiol.* **2**, 1616–1623 (2017).

7. Yen, H. Y. *et al.* PtdIns(4,5)P2 stabilizes active states of GPCRs and enhances selectivity of G-protein coupling. *Nature* **559**, 423–427 (2018).

8. Van Eerden, F. J., Melo, M. N., Frederix, P. W. J. M., Periole, X. & Marrink, S. J. Exchange pathways of plastoquinone and plastoquinol in the photosystem II complex. *Nat. Commun.* **8**, 15214 (2017).

9. Vögele, M., Köfinger, J. & Hummer, G. Hydrodynamics of Diffusion in Lipid Membrane Simulations. *Phys. Rev. Lett.* **120**, (2018).

10. Agostino, M. D., Risselada, H. J., Lürick, A., Ungermann, C. & Mayer, A. A tethering complex drives the terminal stage of SNARE-dependent membrane fusion. *Nature* **551**, 634–638 (2017).

11. Jeena, M. T. *et al.* Mitochondria localization induced self-assembly of peptide amphiphiles for cellular dysfunction. *Nat. Commun.* **8**, 26 (2017).

12. Jiang, Z. *et al.* Subnanometre ligand-shell asymmetry leads to Janus-like nanoparticle membranes. *Nat. Mater.* **14**, 912–917 (2015).

13. Maingi, V. *et al.* Stability and dynamics of membrane-spanning DNA nanopores. *Nat. Commun.* **8**, 14784 (2017).

14. Frederix, P. W. J. M. *et al.* Exploring the sequence space for (tri-)peptide self-assembly to design and discover new hydrogels. *Nat. Chem.* **7**, 30–37 (2015).

15. Bochicchio, D., Salvalaglio, M. & Pavan, G. M. Into the dynamics of a supramolecular polymer at submolecular resolution. *Nat. Commun.* **8**, 147 (2017).

16. Stark, A. C., Andrews, C. T. & Elcock, A. H. Toward optimized potential functions for protein-protein interactions in aqueous solutions: osmotic second virial coefficient calculations using the MARTINI coarse-grained force field. *J. Chem. Theory Comput.* **9**, 4176–4185 (2013).

17. Javanainen, M., Martinez-Seara, H. & Vattulainen, I. Excessive aggregation of membrane proteins in the Martini model. *PLoS One* **12**, e0187936 (2017).

18. Schmalhorst, P. S., Deluweit, F., Scherrers, R., Heisenberg, C.-P. & Sikora, M. Overcoming the Limitations of the MARTINI Force Field in Simulations of Polysaccharides. *J. Chem. Theory Comput.* **13**, 5039–5053 (2017).

19. Alessandri, R. *et al.* Pitfalls of the Martini Model. *J. Chem. Theory Comput.* **15**, 5448–5460 (2019).

20. Uusitalo, J. J., Ingólfsson, H. I., Marrink, S. J. & Faustino, I. Martini Coarse-Grained Force Field: Extension to RNA. *Biophys. J.* **113**, 246–256 (2017).

21. Ben-Naim, A. *Molecular theory of solutions*. (Oxford University Press, 2006).

22. Ploetz, E. A., Bentenitis, N. & Smith, P. E. Kirkwood-Buff integrals for ideal solutions. *J. Chem. Phys.* **132**, 164501 (2010).

23. Zych, A. J. & Iverson, B. L. Synthesis and Conformational Characterization of Tethered, Self-Complexing 1,5-Dialkoxynaphthalene/1,4,5,8-Naphthalenetetracarboxylic Diimide Systems. *J. Am. Chem. Soc.* **122**, 8898–8909 (2000).

24. Gabriel, G. J. & Iverson, B. L. Aromatic oligomers that form hetero duplexes in aqueous solution. *J. Am. Chem. Soc.* **124**, 15174–15175 (2002).

25. Liu, W. *et al.* Structural basis for allosteric regulation of GPCRs by sodium ions. *Science* **337**, 232–236 (2012).

26. Gao, Z. G. & Ijzerman, A. P. Allosteric modulation of A(2A) adenosine receptors by amiloride analogues and sodium ions. *Biochem. Pharmacol.* **60**, 669–676 (2000).

27. Okur, H. I. *et al.* Beyond the Hofmeister Series: Ion-Specific Effects on Proteins and Their Biological Functions. *J. Phys. Chem. B* **121**, 1997–2014 (2017).

28. Dupont, D., Depuydt, D. & Binnemans, K. Overview of the Effect of Salts on Biphasic Ionic Liquid/Water Solvent Extraction Systems: Anion Exchange, Mutual Solubility, and Thermomorphic Properties. *J. Phys. Chem. B* **119**, 6747–6757 (2015).

29. Naert, P., Rabaey, K. & Stevens, C. V. Ionic liquid ion exchange: Exclusion from strong interactions condemns cations to the most weakly

546 interacting anions and dictates reaction equilibrium. *Green Chem.* **20**, 4277–
547 4286 (2018).
548 30. Khan, H. M. *et al.* Capturing Choline-Aromatics Cation-πInteractions in the
549 MARTINI Force Field. *J. Chem. Theory Comput.* **16**, 2550–2560 (2020).
550 31. Tanaka, K., Caaveiro, J. M. M., Morante, K., González-Manãs, J. M. &
551 Tsumoto, K. Structural basis for self-assembly of a cytolytic pore lined by
552 protein and lipid. *Nat. Commun.* **6**, 6337 (2015).
553 32. Huang, G., Willems, K., Soskine, M., Wloka, C. & Maglia, G. Electro-
554 osmotic capture and ionic discrimination of peptide and protein biomarkers
555 with FraC nanopores. *Nat. Commun.* **8**, 935 (2017).
556 33. Alessandri, R., Uusitalo, J. J., De Vries, A. H., Havenith, R. W. A. &
557 Marrink, S. J. Bulk Heterojunction Morphologies with Atomistic Resolution
558 from Coarse-Grain Solvent Evaporation Simulations. *J. Am. Chem. Soc.* **139**,
559 3697–3705 (2017).
560 34. Chiu, M. Y., Jeng, U. S., Su, C. H., Liang, K. S. & Wei, K. H. Simultaneous
561 use of small- and wide-angle X-ray techniques to analyze nanometerscale
562 phase separation in polymer heterojunction solar cells. *Adv. Mater.* **20**, 2573–
563 2578 (2008).
564 35. Petrov, D. & Zagrovic, B. Are Current Atomistic Force Fields Accurate
565 Enough to Study Proteins in Crowded Environments? *PLoS Comput. Biol.* **10**,
566 e1003638 (2014).
567 36. Højgaard, C. *et al.* A Soluble, Folded Protein without Charged Amino Acid
568 Residues. *Biochemistry* **55**, 3949–3956 (2016).

569 37. Ruckenstein, E. & Shulgin, I. L. Effect of salts and organic additives on the
570 solubility of proteins in aqueous solutions. *Advances in Colloid and Interface*
571 *Science* **123**–**126**, 97–103 (2006).
572 38. Zhou, F. X., Cocco, M. J., Russ, W. P., Brunger, A. T. & Engelman, D. M.
573 Interhelical hydrogen bonding drives strong interactions in membrane
574 proteins. *Nat. Struct. Biol.* **7**, 154–160 (2000).
575 39. Zhou, F. X., Merianos, H. J., Brunger, A. T. & Engelman, D. M. Polar
576 residues drive association of polyleucine transmembrane helices. *Proc. Natl.*
577 *Acad. Sci. U. S. A.* **98**, 2250–2255 (2001).
578 40. Grau, B. *et al.* The role of hydrophobic matching on transmembrane helix
579 packing in cells. *Cell Stress* **1**, 90–106 (2017).
580 41. Chen, L., Merzlyakov, M., Cohen, T., Shai, Y. & Hristova, K. Energetics of
581 ErbB1 transmembrane domain dimerization in lipid bilayers. *Biophys. J.* **96**,
582 4622–4630 (2009).
583 42. Artemenko, E. O., Egorova, N. S., Arseniev, A. S. & Feofanov, A. V.
584 Transmembrane domain of EphA1 receptor forms dimers in membrane-like
585 environment. *Biochim. Biophys. Acta* **1778**, 2361–7 (2008).
586 43. Sarabipour, S. & Hristova, K. Glycophorin A transmembrane domain
587 dimerization in plasma membrane vesicles derived from CHO, HEK 293T, and
588 A431 cells. *Biochim. Biophys. Acta - Biomembr.* **1828**, 1829–1833 (2013).
589 44. Chen, L., Novicky, L., Merzlyakov, M., Hristov, T. & Hristova, K.
590 Measuring the Energetics of Membrane Protein Dimerization in Mammalian
591 Membranes. *J. Am. Chem. Soc.* **132**, 3628–3635 (2010).

592 45. Nash, A., Notman, R. & Dixon, A. M. De novo design of transmembrane
593 helix-helix interactions and measurement of stability in a biological membrane.
594 *Biochim. Biophys. Acta - Biomembr.* **1848**, 1248–1257 (2015).
595 46. Finger, C. *et al.* The Stability of Transmembrane Helix Interactions
596 Measured in a Biological Membrane. *J. Mol. Biol.* **358**, 1221–1228 (2006).
597 47. Hong, H., Blois, T. M., Cao, Z. & Bowie, J. U. Method to measure strong
598 protein-protein interactions in lipid bilayers using a steric trap. *Proc. Natl.*
599 *Acad. Sci. U. S. A.* **107**, 19802–19807 (2010).
600 48. Sparr, E. *et al.* Self-association of transmembrane α-helices in model
601 membranes: Importance of helix orientation and role of hydrophobic
602 mismatch. *J. Biol. Chem.* **280**, 39324–39331 (2005).
603 49. MacKenzie, K. R., Prestegard, J. H. & Engelman, D. M. Transmembrane
604 helix dimer: Structure and implications. *Science (80-.).* **276**, 131–133 (1997).
605 50. Trenker, R., Call, M. E. & Call, M. J. Crystal Structure of the Glycophorin A
606 Transmembrane Dimer in Lipidic Cubic Phase. *J. Am. Chem. Soc.* **137**,
607 15676–15679 (2015).
608 51. Domański, J., Sansom, M. S. P., Stansfeld, P. J. & Best, R. B. Balancing
609 Force Field Protein–Lipid Interactions To Capture Transmembrane Helix–
610 Helix Association. *J. Chem. Theory Comput.* **14**, 1706–1715 (2018).
611 52. Souza, P. C. T., Thallmair, S., Marrink, S. J. & Mera-Adasme, R. An
612 Allosteric Pathway in Copper, Zinc Superoxide Dismutase Unravels the
613 Molecular Mechanism of the G93A Amyotrophic Lateral Sclerosis-Linked
614 Mutation. *J. Phys. Chem. Lett.* **10**, 7740–7744 (2019).
615 53. Brini, E. *et al.* Systematic coarse-graining methods for soft matter
616 simulations-a review. *Soft Matter* **9**, 2108–2119 (2013).

54. Foley, T. T., Shell, M. S. & Noid, W. G. The impact of resolution upon entropy and information in coarse-grained models. *J. Chem. Phys.* **143**, 243104 (2015).

55. Wagner, J. W., Dama, J. F., Durumeric, A. E. P. & Voth, G. A. On the representability problem and the physical meaning of coarse-grained models. *J. Chem. Phys.* **145**, 044108 (2016).

56. Wörner, S. J., Bereau, T., Kremer, K. & Rudzinski, J. F. Direct route to reproducing pair distribution functions with coarse-grained models via transformed atomistic cross correlations. *J. Chem. Phys.* **151**, 244110 (2019).

57. Noid, W. G., Chu, J. W., Ayton, G. S. & Voth, G. A. Multiscale coarse-graining and structural correlations: Connections to liquid-state theory. *J. Phys. Chem. B* **111**, 4116–4127 (2007).

58. Wu, Z., Cui, Q. & Yethiraj, A. Driving force for the association of hydrophobic peptides: The importance of electrostatic interactions in coarse-grained water models. *J. Phys. Chem. Lett.* **2**, 1794–1798 (2011).

59. Jin, J., Yu, A. & Voth, G. A. Temperature and Phase Transferable Bottom-up Coarse-Grained Models. *J. Chem. Theory Comput.* (2020). doi:10.1021/acs.jctc.0c00832

60. Yesylevskyy, S. O., Schäfer, L. V, Sengupta, D. & Marrink, S. J. Polarizable water model for the coarse-grained MARTINI force field. *PLoS Comput. Biol.* **6**, e1000810 (2010).

61. Michalowsky, J., Schäfer, L. V., Holm, C. & Smiatek, J. A refined polarizable water model for the coarse-grained MARTINI force field with long-range electrostatic interactions. *J. Chem. Phys.* **146**, 054501 (2017).

641 62. Marrink, S. J. & Tieleman, D. P. Perspective on the Martini model. *Chem.*
642 *Soc. Rev.* **42**, 6801–22 (2013).
643 63. Bruininks, B. M. H., Souza, P. C. T. & Marrink, S. J. A Practical View of
644 the Martini Force Field. in *Methods in Molecular Biology* **2022**, 105–127
645 (Humana Press Inc., 2019).
646 64. Liu, J. *et al.* Enhancing Molecular n-Type Doping of Donor-Acceptor
647 Copolymers by Tailoring Side Chains. *Adv. Mater.* **30**, 1704630 (2018).
648 65. Vazquez-Salazar, L. I., Selle, M., de Vries, A., Marrink, S. J. & Souza, P.
649 C. T. Martini coarse-grained models of imidazolium-based ionic liquids: from
650 nanostructural organization to liquid-liquid extraction. *Green Chem.* **22**, 7376–
651 7386 (2020).
652 66. Souza, P. C. T. *et al.* Protein–ligand binding with the coarse-grained
653 Martini model. *Nat. Commun.* **11**, 1–11 (2020).

FIGURE LEGENDS

Figure 1: Rebalancing R-, S-, and T-beads – (A) Snapshots of simulation boxes containing mixtures of dodecane and water in three resolutions. (**B)** Radial distribution functions (g_{ij}) for all bead combinations in the multi-resolution mixture of water. **(C)** Water-oil transfer free energies (ΔG) computed for around 260 data points using Martini 3. **(D)** Hydrogen bonding potential of mean force (PMF) between nucleobases. On the left, comparison between Martini 2 and 3 for the cytosine-guanine base pair. On the right, comparison of the cytosine-guanine (C-G) and guanine-guanine (G-G) base pairs using Martini 3. In both plots, CHARMM and AMBER atomistic data are also reported[5] for comparison. Errors are estimated with bootstrapping and displayed as transparent shades. In the case of Martini, errors are smaller than 0.1 kJ/mol, and hence are not visible in the graphs.

Figure 2: New chemical bead types, sub-labels, and applications – (A) Self-assembly of aedamers. The left panel shows the dimerization free energies (ΔG_{dim}) of pegylated monomers of 1,5-dialkoxynaphthalene (DAN) and naphthalene diimide (NDI). Errors are estimated with bootstrapping. The right panel shows the self-assembled duplex dimer formed by amide-linked tetramers of NDI (green) and DAN (orange). **(B)** As indicatedby X-ray crystallography[25], sodium ions (charged TQ5 bead) can bind to a buried small cavity in the core of the adenosine A_{2A} receptor. **(C)** Charged Q-beads in Martini 3 follow the classical Hofmeister series, as exemplified by the anion transfer between salt aqueous solutions and organophosphonium-based ionic liquids (right panel). Errors in the average anion transfer percentage are estimated by block averaging. **(D)** Preferential cation-π interaction between choline groups (Q1 bead) of phosphatidylcholine lipids and aromatic residues of the *Bacillus thuringiensis* phosphatidylinositol-specific phospholipase C (*Bt*PI-PLC). The depth of insertion of each amino acid of *Bt*PI-PLC is in very good agreement with the insertion obtained from an atomistic MD simulation[30].

Figure 3: Improving packing, cavities and reducing protein stickiness – (**A**) Hydration of Fragaceatoxin C (FraC) nanopore inserted in a lipid bilayer. (**B**) Scattering profiles and a Martini 3 snapshot of a bulk heterojunction morphology of poly(3-hexyl-thiophene) (P3HT, in red) and phenyl-C61-butyric acid methyl ester (PCBM, in blue) formed after solvent evaporation and annealing simulations. *I(q)* corresponds to scattering intensity and *q* is the reciprocal space vector. (**C**) Aggregation levels of the soluble proteins villin headpiece and the modified EXG-CBM in different salt concentrations. (**D**) Aggregation levels of polyleucine helices in POPC and DLPC bilayers. Errors in the average monomer percentage of **(C)** and **(D)** are estimated by block averaging. (**E**) Dimerization of transmembrane helices. Left panel shows a comparison between experimental and calculated values for the mole fraction standard Gibbs free energy of dimerization (ΔG_{ass}^{X}) of the following transmembrane protein domains: ErbB1, EphA1, WALP23 and GpA. Simulation errors are estimated with bootstrapping while experimental data was obtained in the literature[41-48]. In the case of GpA, error was estimated by the mean absolute error of four independent experimental data[43-47]. A comparison between experimental and simulated binding modes of GpA is highlighted in the right panel. The experimental structure was taken from solution NMR in micelles (PDB code AFO)[49]. Near identical experimental structures were obtained by ssNMR in nanodiscs and X-ray crystallography in a lipid cubic phase[49–51].

ONLINE METHODS

1) CG models

CG mappings of small molecules were initially inspired by the standard Martini 2 models, when they were available. Due to the well-balanced properties of the regular (R), small (S), and tiny (T) beads in Martini 3, the CG models now follow more specific rules for mapping. For instance, over-representing 3-to-1 or 2-to-1 fragments by the usage of R-beads is always avoided. Aromatic rings without substituents are composed of T-beads and, in case of substituents, S-beads are used. Aliphatic rings without substituents are usually based on S-beads, which better reproduce their molecular shape. More technical details about the mapping rules and bead types used are given in the **Supplementary Notes**, **sections C1** and **C3**. As in the previous version of Martini[5,20,67–69], bonded parameters are based on atomistic simulations or high-resolution experimental data. The main difference in Martini 3 lies in the protocol to derive bond lengths, which are now based on matching overall volume and shape of the molecules (**Supplementary Notes, section C2**). In this spirit, the bonded parameters of the protein models were also slightly modified from the standard Martini 2.2 values[68,70], including the addition of side chain corrections[71], based on experimental reference structures. Backbone bead types do not depend on the secondary structure anymore, but are now represented by P2 beads, except for proline (SP1a), alanine (SP2, with an additional bead for the side chain) and glycine (SP1). Adapted versions of Gō-like models[72] or Elastic Networks[73] were used to maintain the tertiary protein structure. All CG protein models were constructed using *Martinize2,* described in **Supplementary Codes, section H1**. Lipid

mapping was inspired by the previous Martini model[74–77], but now following the Martini 3 rules for mapping and also with adaptations in the bonded parameters inspired by the "extensible model" of Carpenter *et al.*[78].

2) General setup for CG MD simulations and Analysis

Settings for the CG simulations followed, in general, the "new" Martini set of simulation parameters[79] using the leap-frog algorithm[80] for integrating the equations of motion. The Verlet neighbor search algorithm[81] is used to update the neighbor list every 20 steps with a buffer tolerance of 0.005 $kJ \cdot mol^{-1} \cdot ps^{-1}$. For the Lennard-Jones terms, we used a cutoff scheme with a value of 1.1 nm and the Verlet cutoff scheme[82] for the potential-shift. Long range electrostatic interactions were treated with reaction field[83] or Particle Mesh Ewald (PME)[84], with relative permittivity set to ϵ_r=15 and a cutoff value of 1.1 nm. Reaction field was used for most of the systems, except the ones explicitly mentioning PME. Periodic boundary conditions were used in all three dimensions. For the production simulations, the velocity rescaling thermostat[85] (coupling time constant of 1.0 ps) and the Parrinello-Rahman barostat[86] (coupling time constant of 12.0 ps) were employed to maintain temperature and pressure, respectively. Except for equilibration runs, a time step of 20 fs was used for all systems. CG simulation settings are available as input files for GROMACS on the Martini portal http://cgmartini.nl. GROMACS 2016.x and 2018.x were used to run all the MD simulations[87,88]. For automated running and managing the Martini 3 simulations, we provide an updated version of *Martinate*[89,90], described in **Supplementary Codes, section H2.** All the analysis were performed using *gmx analysis tools* (GROMACS 2016 and 2018)[87,88], VMD

753 1.9.4a12[91], xmgrace (5.1.25) and MDAnalysis[92]. The graphs were plotted
754 using Excel 2016, xmgrace (5.1.25) and gnuplot (5.2). Figures were compiled
755 using VMD 1.9.4a12 and Inkscape 1.1.
756
757 **3) Parameter calibration, tests and validation**
758 In order to parametrize the LJ parameters of single beads and also test the
759 Martini 3 CG models, many molecular systems and methods were used in this
760 work. The overall iterative approach was not based in rigorous separation of
761 calibration and validation groups. As Martini is based on pair interactions, it is
762 hard to find simple systems that cover enough points in the interaction matrix
763 for all bead size combinations. So, complex systems are not only used for
764 validation but can be part of the calibration. The tests performed were
765 separated in “tiers”, which represent systems with different level of complexity.
766 In “tier 0”, isolate beads and simple-molecules are mainly used for calibration
767 of LJ parameters, with balance of different bead sizes and thermodynamics
768 data (e.g. liquid-liquid partitioning and miscibility) used as main targets. In the
769 intermediate “tier 1”, bilayer properties are checked, together with qualitative
770 tests, applied to systems like soluble and transmembrane proteins. These
771 qualitative tests are designed as “yes-or-no” questions to evaluate the overall
772 quality of the force field. At the same time, some points in the interaction
773 matrix were also tested and fine-tuned here. In the final “tier 2", quantitative
774 tests involving complex systems are performed, including comparisons with
775 experimental or atomistic simulation data. Here most of the system are
776 considered validation. For a complete overview of the parametrization
777 strategy used, see the **Supplementary Notes, section B**. The

Supplementary Notes, section D provide details of the specific systems and methods used in the tests performed to parametrize and validate the new Martini 3 LJ parameters. Further information on research design is available in the Life Sciences Reporting Summary linked to this article.

DATA AVAILABILITY

Force-field parameters and procedures (e.g. tutorials) are publicly available at http://cgmartini.nl. Simulation Data (e.g. trajectories) supporting the results of this paper are available from the corresponding authors upon reasonable request.

CODE AVAILABILITY

Martinize2 (for which the manuscript is in preparation) and *Martinate* codes used in this work are publicly available at https://github.com/marrink-lab/. For a more detailed information, see **Supplementary Codes**, **section H**.

REFERENCES

67. López, C. A. *et al.* Martini Coarse-Grained Force Field: Extension to Carbohydrates. *J. Chem. Theory Comput.* **5**, 3195–3210 (2009).

68. Monticelli, L. *et al.* The MARTINI Coarse-Grained Force Field: Extension to Proteins. *J. Chem. Theory Comput.* **4**, 819–834 (2008).

69. Grunewald, F., Rossi, G., de Vries, A. H., Marrink, S. J. & Monticelli, L. Transferable MARTINI Model of Poly(ethylene Oxide). *J. Phys. Chem. B* **122**, 7436–7449 (2018).

70. de Jong, D. H. *et al.* Improved Parameters for the Martini Coarse-Grained Protein Force Field. *J. Chem. Theory Comput.* **9**, 687–97 (2013).

71. Herzog, F. A., Braun, L., Schoen, I. & Vogel, V. Improved Side Chain Dynamics in MARTINI Simulations of Protein–Lipid Interfaces. *J. Chem. Theory Comput.* **12**, 2446–2458 (2016).

72. Poma, A. B., Cieplak, M. & Theodorakis, P. E. Combining the MARTINI and Structure-Based Coarse-Grained Approaches for the Molecular Dynamics Studies of Conformational Transitions in Proteins. *J. Chem. Theory Comput.* **13**, 1366–1374 (2017).

73. Periole, X., Cavalli, M., Marrink, S.-J. & Ceruso, M. A. Combining an Elastic Network With a Coarse-Grained Molecular Force Field: Structure, Dynamics, and Intermolecular Recognition. *J. Chem. Theory Comput.* **5**, 2531–2543 (2009).

74. Marrink, S. J., Risselada, H. J., Yefimov, S., Tieleman, D. P. & de Vries, A. H. The MARTINI force field: coarse grained model for biomolecular simulations. *J. Phys. Chem. B* **111**, 7812–7824 (2007).

820 75. Wassenaar, T. A., Ingólfsson, H. I., Böckmann, R. A., Tieleman, D. P. &
821 Marrink, S. J. Computational Lipidomics with *insane*: A Versatile Tool for
822 Generating Custom Membranes for Molecular Simulations. *J. Chem. Theory*
823 *Comput.* **11**, 2144–2155 (2015).
824 76. Melo, M. N., Ingólfsson, H. I. & Marrink, S. J. Parameters for Martini
825 sterols and hopanoids based on a virtual-site description. *J. Chem. Phys.* **143**,
826 243152 (2015).
827 77. López, C. A., Sovova, Z., van Eerden, F. J., de Vries, A. H. & Marrink, S.
828 J. Martini Force Field Parameters for Glycolipids. *J. Chem. Theory Comput.* **9**,
829 1694–1708 (2013).
830 78. Carpenter, T. S. *et al.* Capturing Phase Behavior of Ternary Lipid Mixtures
831 with a Refined Martini Coarse-Grained Force Field. *J. Chem. Theory Comput.*
832 **14**, 6050–6062 (2018).
833 79. de Jong, D. H., Baoukina, S., Ingólfsson, H. I. & Marrink, S. J. Martini
834 straight: Boosting performance using a shorter cutoff and GPUs. *Comput.*
835 *Phys. Commun.* **199**, 1–7 (2016).
836 80. Hockney, R. W., Goel, S. P. & Eastwood, J. W. Quiet high-resolution
837 computer models of a plasma. *J. Comput. Phys.* **14**, 148–158 (1974).
838 81. Páll, S. & Hess, B. A flexible algorithm for calculating pair interactions on
839 SIMD architectures. *Comput. Phys. Commun.* **184**, 2641–2650 (2013).
840 82. Verlet, L. Computer 'experiments' on classical fluids. I. Thermodynamical
841 properties of Lennard-Jones molecules. *Phys. Rev.* **159**, 98–103 (1967).
842 83. Tironi, I. G., Sperb, R., Smith, P. E. & Van Gunsteren, W. F. A generalized
843 reaction field method for molecular dynamics simulations. *J. Chem. Phys.*
844 **102**, 5451–5459 (1995).

84. Essmann, U. *et al.* A smooth particle mesh Ewald method. *J. Chem. Phys.* **103**, 8577–8593 (1995).

85. Bussi, G., Donadio, D. & Parrinello, M. Canonical sampling through velocity rescaling. *J. Chem. Phys.* **126**, 014101 (2007).

86. Parrinello, M. & Rahman, A. Polymorphic transitions in single crystals: A new molecular dynamics method. *J. Appl. Phys.* **52**, 7182–7190 (1981).

87. Abraham, M. J. *et al.* GROMACS: High performance molecular simulations through multi-level parallelism from laptops to supercomputers. *SoftwareX* **1–2**, 19–25 (2015).

88. Van Der Spoel, D. *et al.* GROMACS: Fast, flexible, and free. *J. Comput. Chem.* **26**, 1701–1718 (2005).

89. Wassenaar, T. A., Ingólfsson, H. I., Prieß, M., Marrink, S. J. & Schäfer, L. V. Mixing MARTINI: Electrostatic coupling in hybrid atomistic-coarse-grained biomolecular simulations. *J. Phys. Chem. B* **117**, 3516–3530 (2013).

90. Wassenaar, T. A. *et al.* High-Throughput Simulations of Dimer and Trimer Assembly of Membrane Proteins. The DAFT Approach. *J. Chem. Theory Comput.* **11**, 2278–91 (2015).

91. Humphrey, W., Dalke, A. and Schulten, K. VMD - Visual Molecular Dynamics. *J. Molec. Graph.* **14**, 33–38 (1996).

92. Gowers, R. J. *et al.* MDAnalysis: A Python Package for the Rapid Analysis of Molecular Dynamics Simulations. In *Proc. 15th Python Sci. Conference* 98–105 (2016).

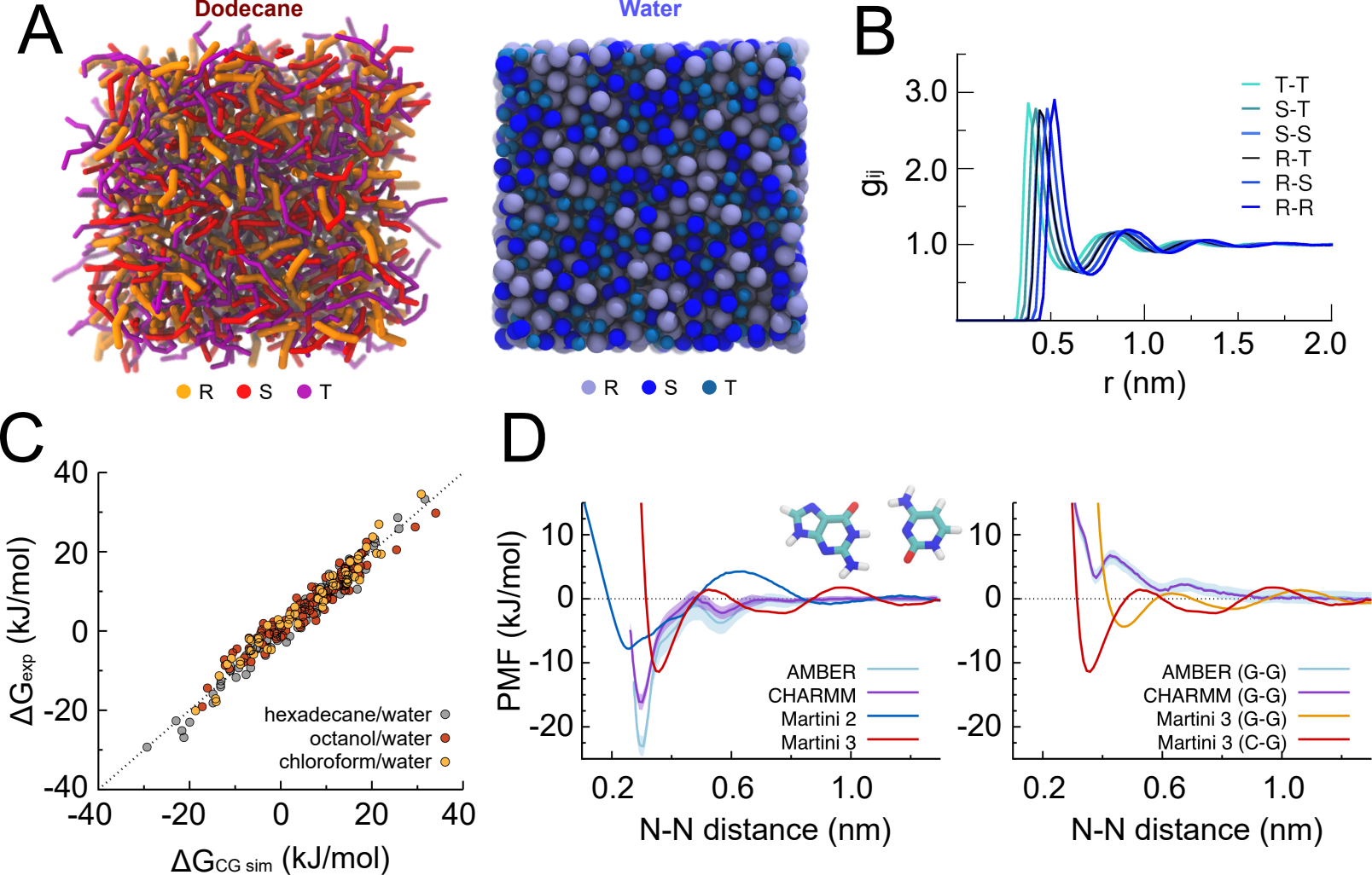
A
Dodecane
Water
R S T
R S T
B
3.0
2.0
1.0
g_{ij}
T-T
S-T
S-S
R-T
R-S
R-R
0.5 1.0 1.5 2.0
r (nm)
C
40
20
0
-20
-40
ΔG_{exp} (kJ/mol)
hexadecane/water
octanol/water
chloroform/water
-40 -20 0 20 40
$\Delta G_{CG\ sim}$ (kJ/mol)
D
10
0
-10
-20
PMF (kJ/mol)
AMBER
CHARMM
Martini 2
Martini 3
0.2 0.6 1.0
N-N distance (nm)
AMBER (G-G)
CHARMM (G-G)
Martini 3 (G-G)
Martini 3 (C-G)
0.2 0.6 1.0
N-N distance (nm)

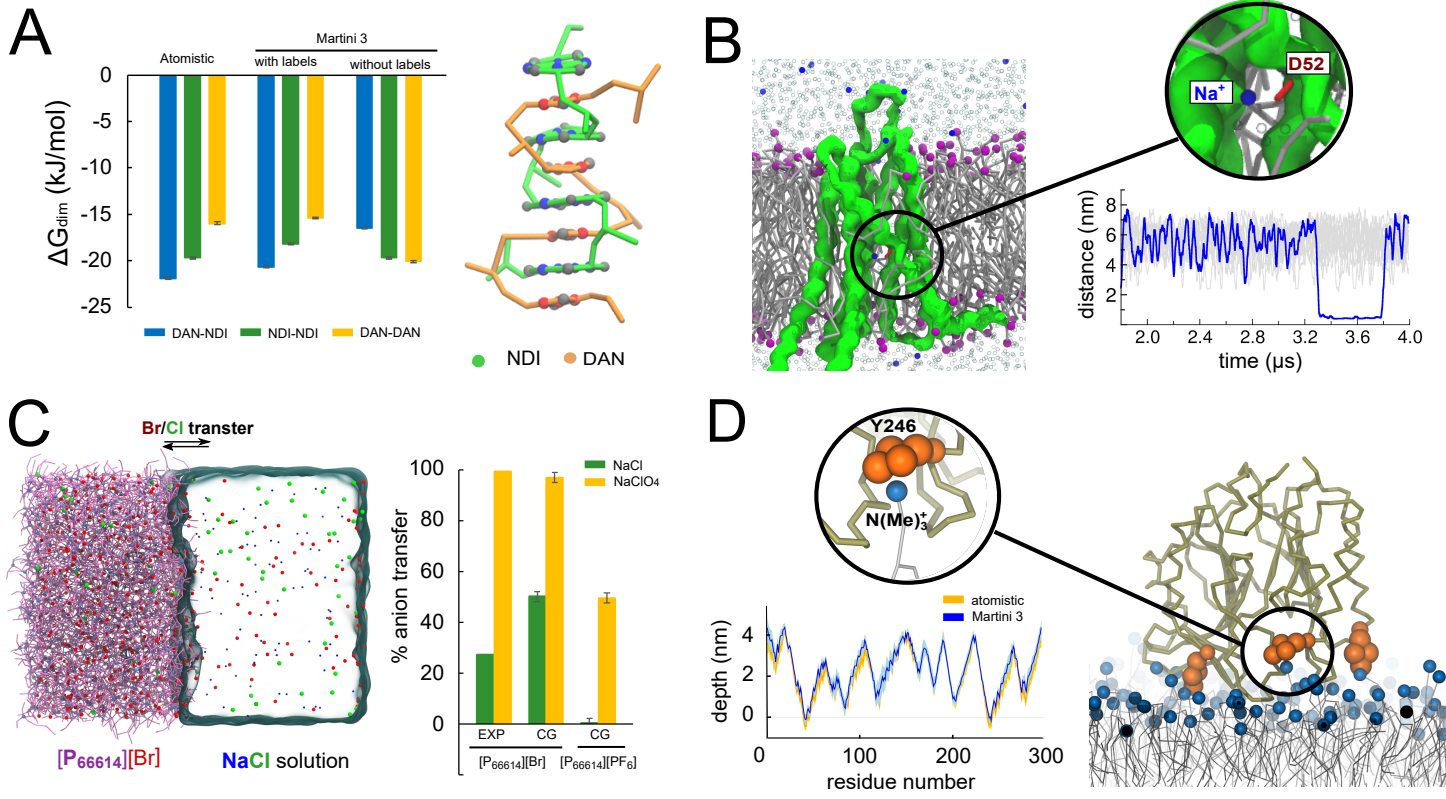
A
Martini 3
Atomistic
with labels
without labels
0
-5
-10
-15
-20
-25
ΔGdim (kJ/mol)
DAN-NDI
NDI-NDI
DAN-DAN
NDI
DAN
B
Na+
D52
distance (nm)
8
6
4
2
2.0
2.4
2.8
3.2
3.6
4.0
time (μs)
C
Br/Cl transter
[P66614][Br]
NaCl solution
% anion transfer
100
80
60
40
20
0
NaCl
NaClO4
EXP
CG
CG
[P66614][Br]
[P66614][PF6]
D
Y246
N(Me)3+
atomistic
Martini 3
depth (nm)
4
2
0
0
100
200
300
residue number

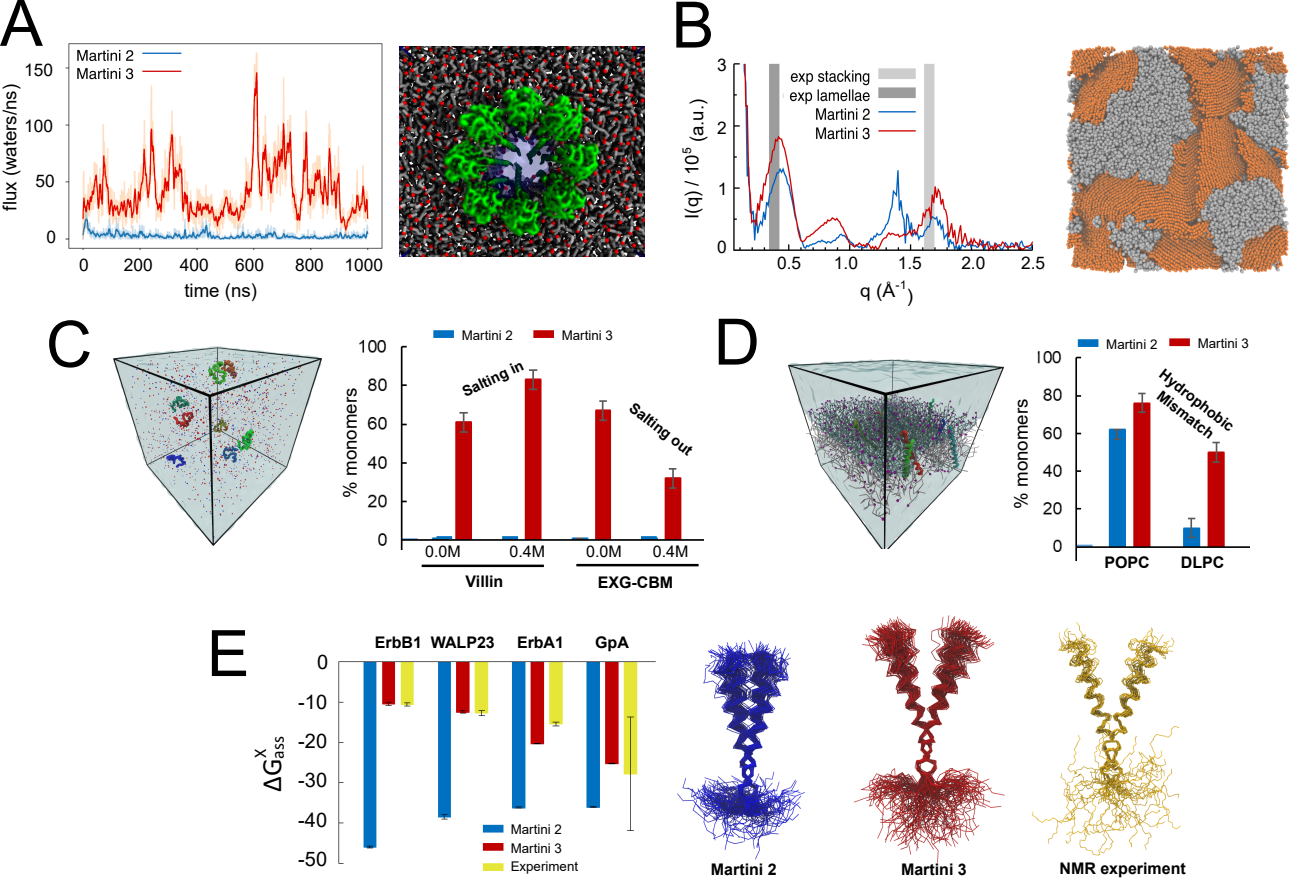
A
Martini 2
Martini 3
flux (waters/ns)
150
100
50
0
0
200
400
600
800
1000
time (ns)
B
exp stacking
exp lamellae
Martini 2
Martini 3
I(q) / 10^5 (a.u.)
3
2
1
0
0.5
1.0
1.5
2.0
2.5
q (Å^-1)
C
Martini 2
Martini 3
% monomers
100
80
60
40
20
0
Salting in
Salting out
0.0M
0.4M
0.0M
0.4M
Villin
EXG-CBM
D
Martini 2
Martini 3
% monomers
100
80
60
40
20
0
Hydrophobic
Mismatch
POPC
DLPC
E
ErbB1
WALP23
ErbA1
GpA
ΔG^X_ass
0
-10
-20
-30
-40
-50
Martini 2
Martini 3
Experiment
Martini 2
Martini 3
NMR experiment